



Nonlinear Finite Element Analysis of Steel Fiber Reinforced Concrete Deep Beams With and Without Opening

Hayder Qais Majeed
Asst. lecturer, College of engineering
Baghdad University, Iraq
E-mail: hayderqs@yahoo.com

Abstract

This paper presents a nonlinear finite element modeling and analysis of steel fiber reinforced concrete (SFRC) deep beams with and without openings in web subjected to two- point loading. In this study, the beams were modeled using ANSYS nonlinear finite element software. The percentage of steel fiber was varied from 0 to 1.0%. The influence of fiber content in the concrete deep beams has been studied by measuring the deflection of the deep beams at mid- span and marking the cracking patterns, compute the failure loads for each deep beam, and also study the shearing and first principal stresses for the deep beams with and without openings and with different steel fiber ratios. The above study indicates that the location of openings and the amount steel fiber are affects to the behavior and strength of deep beams. And also when the results of the experiments taken from the literature were compared with the results obtained from the beam modeled with ANSYS finite element program, it was shown that the results of computer model gave similar results to the experimental behavior.

Keywords: Deep beams, Steel fibers, Beam Web openings, SFRC Beams, Ansys

-:

(SFRC)

.1.0% 0

. ANSYS

ANSYS

الكلمات الرئيسية: الجسور العميقة، الاليف الفولاذية، الفتحات الجذعية، الجسور المسلحة المقواة بالاياف الفولاذية، الانسز

1. Introduction

For reinforced concrete, improvement of calculation methods and analysis of behavior by either creating a model on computer or counting with analytical calculation methods are used extensively in recent years. The behavior of a reinforced concrete element is generally observed by conducting experiment on laboratory environment; but this process considerably takes up much time. The studies are limited due to the problems in providing the materials and the proper conditions to conduct the experiments and scarcity of usage of materials which are constituted according to certain size and number of elements. Modeling of all these processes unlimitedly in computer is dependent on the capacity of the computer being used. While modeling on the computer, properties and limit conditions of materials should be defined properly and completely [Lawrance KL 2002].

ANSYS finite element program is chosen for this study. Finite element method is a numeric method which can solve complex and difficult physical problems) with acceptable approximation.

As concrete is a material showing nonlinear behavior during loading, it is modeled in such a way that it will show a nonlinear behavior with ANSYS finite element program [Barbosa AF, Riberio 2004].

Deep beams are often used as structural members in Civil Engineering works. In many cases, web openings are required to provide for services or for access. Because of the geometric proportions of deep beams, their strength is usually controlled by shear rather than flexure, if normal amounts of reinforcements are provided. A proliferation of new developments in steel fiber reinforced concrete technology has greatly extended the range of applications. The application currently depends on the ingenuity of the designer and builder taking advantage of the improved static and dynamic tensile strength, ductility, energy – absorbing characteristics, abrasion resistance, and fatigue strength of this material of construction [Mansur,

M.A1982, and Vengatachalapathy.V 2010].

The uniform dispersion of steel fiber throughout the concrete provided isotropic strength properties which are not exhibited by conventionally reinforced concrete. A number of investigations are being carried out on the behavior of fiber reinforced composites. Since 1972, a number of experimental and analytical investigations have been carried out to study the behavior and collapse loads of deep beams with and without web opening [Leonhardt,F 1972].

The openings are usually provided in such beams to have an access for utility ducts without further increases in ceiling head room. As the usage of those beams with or without openings increases, it becomes imperative that the design criteria of such beams is widely tested and established [Vengatachalapathy.V 2010].

2. Experimental Study

Vengatachalapathy et al. (2010) [Vengatachalapathy.V 2010] modeled of simply supported nine concrete deep beams of dimensions 750mm ×350mm×75mm thickness were tested to destruction by applying gradually increased load. The percentage of steel fiber was varied from 0 to 1.0.

3. Finite Element Modeling of Steel Reinforcement and Steel Fiber

Tavarez discusses three techniques that exist to model steel reinforcement in finite element models for reinforced concrete is shown in figure 1 the discrete model, the embedded model, and the smeared model [Tavarez (2001)]. In this study the main and web steel reinforcement are modeled as discrete and embedded, and the steel fiber modeled as smeared model.

4. The Finite Element Model

The material models used for transferring material properties of the specimen to the designed computer program are given in this section. ANSYS 11, finite element program is used for modeling. Material properties of concrete, reinforcement and

adhesive are defined and entered as data in the model. Some criteria given below are based on to define the material properties:

4.1. Reinforced Concrete

The solid element (Solid 65) has eight nodes with three degrees of freedom at each node and translations in the nodal x, y, and z directions. The element is capable of plastic deformation, cracking in three orthogonal directions, and crushing. The geometry and node locations for this element type are shown in figure 3. Smeared cracking approach has been used in modeling the concrete in the present study [ANSYS, Inc 2006].

The geometry and node locations for Link 8 element used to model the steel reinforcement are shown in figure 4. Two nodes are required for this element. Each node has three degrees of freedom, translations in the nodal x, y, and z directions. The element is also capable of plastic deformation [ANSYS, Inc 2006].

4.2. Steel Plates

An eight-node solid element, Solid45, was used for the steel plates at support and load locations. The element is defined with eight nodes having three degrees of freedom at each node and translations in the nodal x, y, and z directions. The geometry and node locations for this element type are shown in Figure 4. Steel plate modeled using Solid45 elements, was added at the support locations in order to avoid stress concentration problems and to prevent localized crushing of concrete elements near the supporting points and load application locations. This provided a more even stress distribution over the support area [ANSYS, Inc 2006].

5. Real Constant and Material Properties:-

The real constants for these models are shown in Table 1. Note that individual elements contain different real constants. No real constant set exists for the Solid45 element. In this study the volume ratio of the real constant for solid 65 element varying from 0% - 1.0% depending on the steel fiber ratio imbedded in concrete, and

the material number of steel fiber indicated in table 2.

Parameters needed to define the material models can be found in Table 2. The Solid65 element requires linear isotropic and multi-linear isotropic material properties to properly model concrete. The multi-linear isotropic material uses the von Mises failure criterion along with the Willam and Warnke (1975) model to define the failure of the concrete. EX is the modulus of elasticity of the concrete (E_c), and PRXY is the Poisson's ratio (μ). The compressive uniaxial stress-strain relationship for the concrete model was obtained using the following equations to compute the multi-linear isotropic stress-strain [Saifullah, et al 2011].

$$f = \frac{E_c \varepsilon}{1 + \left(\frac{\varepsilon}{\varepsilon_0}\right)^2} \quad (1)$$

$$\varepsilon_0 = \frac{2f_c^-}{E_c} \quad (2)$$

$$E_c = \frac{f}{\varepsilon} \quad (3)$$

Where:

f = stress at any strain ε , N/mm²

ε = strain at stress f

ε_0 = strain at the ultimate compressive strength, f_c^- .

The multi-linear curve is used to help with convergence of the nonlinear solution algorithm. Figure 5 shows the stress-strain relationship used for this study and is based on work done by Vengatachalapathy et al. (2010). Nonlinear model curve Point 1, defined as $0.3 f_c^-$ is calculated in the linear range Equation 3. Other points are calculated from Equation 1 with ε_0 obtained from Equation 2. Last point is defined at f_c^- and $\varepsilon_0=0.003$ mm/mm indicating traditional crushing strain. Figures 6 and 7 show the stress- strain curves for the main steel reinforcement and web reinforcement respectively.

6. Modeling:-

The beam specimen consists of 350 x 75mm section of 750 mm long. The geometry of these samples and the location of the openings are shown in figure 8. Due to symmetry half of the beam is modeling as shown in figure 9. The bond between steel reinforcement and concrete was assumed as perfect in the modeling of RC control beam specimen. Each beam contained two steel rods of 16mm diameter of 415 N/mm² yield strength were used as the main tension, and web reinforcement consisting of two layers of welded wire fabric of 3.3mm diameter and 50mm on centers having yield strength of 300 N/mm², as shown in figure 10. The FE mesh for the beam model is shown in figure 11.

7. Non-Linear Solution

In this study the total load applied was divided into a series of load increments (or) load steps. Newton -Raphson equilibrium iterations provide convergence at the end of each load increment within tolerance limits. The automatic time stepping in the ANSYS program predicts and controls load step sizes for which the maximum and minimum load step sizes are required. After attempting many trials the number of load steps, minimum and maximum step sizes was determined. During concrete cracking, steel yielding and ultimate stage in which large numbers of cracks occur the loads were applied gradually with smaller load increments.

8. Discussions of Results

8.1 Load Deflection Curves

The experimental carried by Vengatachalapathy et al. (2010) and ansys load-deflection curves obtained for the beams are illustrated in figures 12, 13, and 14. The curves show good agreement in finite element analysis with the experimental results throughout the entire range of behavior and failure mode. Figure 15 shows deferent ratios of steel fiber content, in this study the ratios of 0.25% and 0.5% are added to the results to make comparison with more steel fiber ratios, for all beams the finite element model is stiffer than the actual beam in the

linear range. Several factors may cause the higher stiffness in the finite element models. The bond between the concrete and steel reinforcing is assumed to be perfect (no slip) in the finite element analyses, but for the actual beams the assumption would not be true slip occurs, therefore the composite action between the concrete and steel reinforcing is lost in the actual beams. After the initiation of flexural cracks, the beam stiffness was reduced and the linear load –deflection behavior ended when the internal steel reinforcement began to yield.

8. 2 Crack Pattern

The ANSYS program records a crack pattern at each applied load step. Figure 16 shows evolutions of crack patterns developing for each beam at the last loading step. ANSYS program displays circles at locations of cracking or crushing in concrete elements. Cracking is shown with a circle outline in the plane of the crack, and crushing is shown with an octahedron outline. The first crack at integration point is shown with a red circle outline, the second crack with a green outline, and the third crack with a blue outline [ANSYS, Inc 2006].

8. 3 Failure Load

The failure load obtained from the numerical solution for all beams is slightly smaller than experimental load. The final loads for the finite element models are the last applied load step before the solution diverges due to numerous cracks and large deflections. Table 1 shows comparison between the ultimate loads of the experimental beams and the final loads from the finite element models for deep beams with deferent ratios of steel content with and without opening, and also show the percentage of increase in the final load with the different values of steel fiber.

8.4 Shearing and Principal Stresses

Figures (17-25) show the shearing and 1st principal stress at first crack for the deep beams with and without opening and with steel fiber ratios varying from (0- 1.0%). For the solid deep beam the bearing load at the 1st crack increase with increases in the steel fiber percentage as shown in figures



(17-19 a), whereas for deep beam with openings the bearing load at 1st crack is remained constant with increase in the steel fiber ratios as shown in figures (20-25 a). For the solid deep beam the shearing stress transfer from the point load to the support as fusiform shape, when the way between loading point and support intersects with the opening the shearing stress transform to the support come around the opening as shown in figures (17-25 b). For the solid deep beam the largest stress appears at the mid-span at the 1st crack happened as shown in figures (17-19 c), and for deep beam with opening the big stress appears at the edges of the opening along loading point as shown in figures (20-25 c).

9. Conclusions

- The general conclusion is that 3D ANSYS modeling is able to properly simulate the nonlinear behavior of the steel fiber reinforced concrete Deep Beams With and Without Openings.
- In simple, ANSYS is a rapid way compared with experimental test.
- The general behavior of the finite element models shows good agreement with observations and data from the experimental beam tests of the others.
- The results obtained demonstrate that web openings may be provided in the compression zone of the beams and fiber content of 0.75% by volume may be added to improve the strength of the structure. The openings in the tension zone weaken the beam. And Fiber content of 0.75% by volume of the beam improves the ultimate load.
- The percentage of increase in load capacity at the 1st crack for the solid deep beam is 32.3% when 0.75% steel fiber added, and 33.3% for 1.0% steel fiber added therefore use 0.75% fiber give good strength and more economic than 1.0% steel fiber.
- No significant increase in the load capacity at the 1st crack for the deep beam with opening.

10. References

- ANSYS, Inc., "ANSYS Help", Release 11.0, Documentation, Copyright 2006
- Bangash, M.Y.H. (1989), Concrete and Concrete Structures: Numerical Modeling and Applications, London, England: Elsevier Science Publishers Ltd.
- Barbosa AF, Riberio GO (2004). Analysis of reinforced concrete structures using ANSYS nonlinear concrete model. Computer. Mech. 1(8): pp. 1-7.
- Barzegar, F., Maddipudi, S. (1997), "Three – Dimensional Modeling of Concrete structures. I". Plain Concrete Journal of Structural Engineering, pp.1339-1346.
- Leonhardt, F. H.A.R.de Paiva and C.P.Siess 1972, Discussion of :Strength and behavior of deep beams in shear. Proceedings of the American Society of Civil Engineers. Vol.92, No. 2
- Lawrance KL (2002). ANSYS Tutorial Release 7.0 and 6.1, SDC Publications, Canonsburg, 1.1- 2.25.
- Mansur, M.A, and Alwis, W.A.M., 1982, Reinforced fiber concrete deep beams with web openings, The international journal of cement composites and lightweight concrete, Vol.6., No.4.
- Saifullah, M.A. Hossain, (2011) " Nonlinear Analysis of RC Beam for Different Shear Reinforcement Patterns by Finite Element Analysis". International Journal of Civil & Environmental Engineering IJCEE-IJENS Vol: 11 No: 01 pp.86-98.
- Tavarez, F.A., (2001), "Simulation of Behavior of Composite Grid Reinforced Concrete Beams Using Explicit Finite Element Methods," Master's Thesis, University of Wisconsin-Madison, Madison, Wisconsin.-
- Vengatachalapathy.V, Ilangoan.R 2010, A Study on Steel Fibre Reinforced Concrete Deep Beams With and without Openings. International Journal of Civil and Structural Engineering Volume 1, No 3, 2010 pp.509-517.

Table 1. Real constant for model

Real Constant set	Element Type		Real Constant for Rebar 1	Real Constant for Rebar 2	Real Constant for Rebar 3
1	Solid 65		0	0	0
		Material Number	0	0	0
		Volume Ratio	0	0	0
		Orientation Angle	0	0	0
		Orientation Angle	0	0	0
2	Link8	Cross-Sectional Area (mm ²)	201		
		Initial Strain (mm/mm)	0		
3	Link8	Cross-Sectional Area (mm ²)	8.56		
		Initial Strain (mm/mm)	0		

Table 2. Material Models for the Calibration Model

Material Model Number	Element Type	Material Properties	
		Linear Isotropic	
		EX (MPa)	29,715
		PRXY	0.2
		Multilinear Isotropic	
		Strain (mm/mm)	Stress (MPa)
		0.0002736	8.13
		0.0004	11.34
		0.0008	20
		0.0012	24.89
		0.0016	26.87
		0.001824	27.1
		0.003	27.1
		Concrete	
		ShrCf-Op	0.2
		ShrCf-Cl	0.8
		UnTensSt	2.57
		UnCompSt	-1
		BiCompSt	0
		HydroPs	0
BiCompSt	0		



		UnTensSt	0
		TenCrFac	0
2	Link 8	Linear Isotropic	
		EX (MPa)	200,000
		PRXY	0.3
		Bilinear Isotropic	
		Yield Stress (MPa)	415
		Tangent Modulus (MPa)	0
3	Link 8	Linear Isotropic	
		EX (MPa)	200,000
		PRXY	0.3
		Bilinear Isotropic	
		Yield Stress (MPa)	300
		Tangent Modulus (MPa)	0
4	Solid 45	Linear Isotropic	
		EX (MPa)	200,000
		PRXY	0.3
5	Link 8	Linear Isotropic	
		EX (MPa)	200,000
		PRXY	0.3
		Bilinear Isotropic	
		Yield Stress (MPa)	1100
		Tangent Modulus (MPa)	0

Table 3. Experimental and Analytical Ultimate Loads for Deep beams

Opening Position	Fiber 0%			Fiber 0.75%				Fiber 1.0%			
	Experimental load(kN) <small>[Vengatachalapathy, V 2010]</small>	Analytical load(kN)	% Difference	Experimental load(kN) <small>[Vengatachalapathy, V 2010]</small>	Analytical load(kN)	% Difference	% Increase in the Ultimate Load	Experimental load(kN) <small>[Vengatachalapathy, V 2010]</small>	Analytical load(kN)	% Difference	% Increase in the Ultimate Load
Without web opening (WWBO)	204.50	183.56	10.2	238.14	218.62	8.20	16.04	220.23	212.76	3.39	13.72
Web opening at A (WBOA)	173.00	163.76	5.34	234.36	211.23	9.87	22.47	209.44	187.26	10.6	12.55
Web opening position at B (WBOB)	165.30	150.23	9.12	190.51	183.11	3.88	17.96	180.99	167.77	7.3	10.45

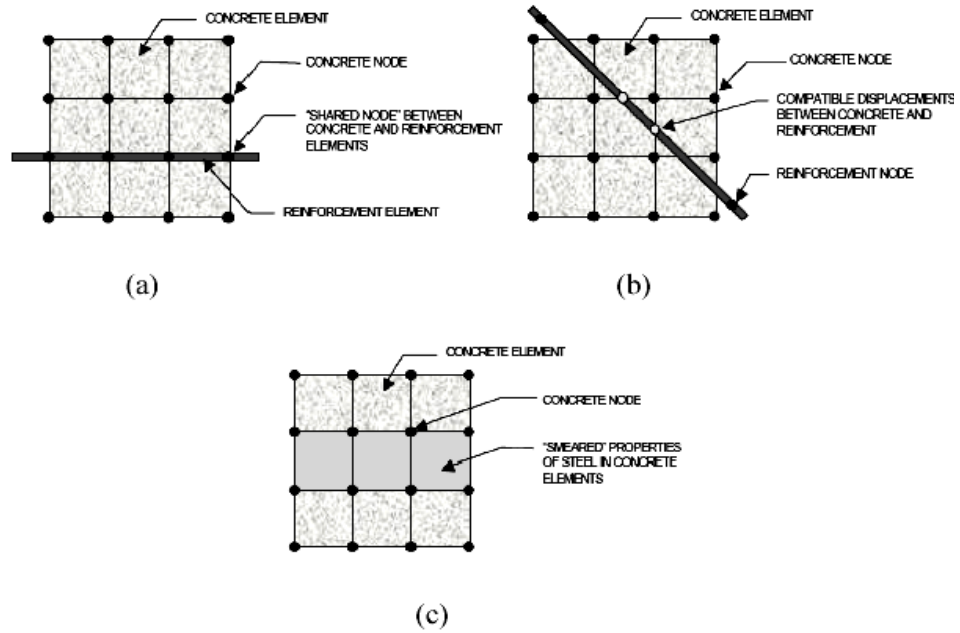


Fig. 1: Models for Reinforcement in Reinforced Concrete (Tavarez 2001): (a) discrete; (b) embedded; and (c) smeared

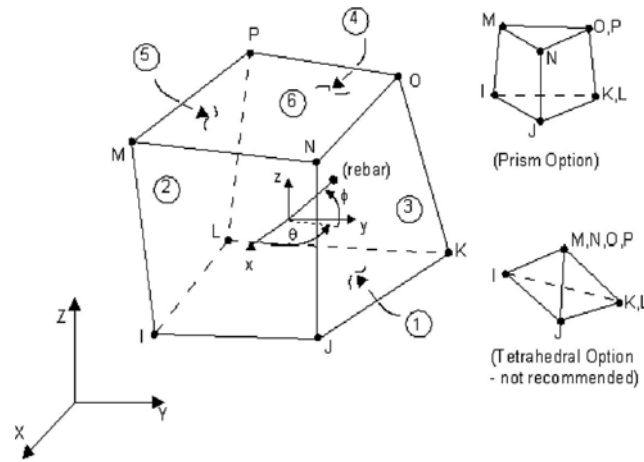


Fig. 2: Solid 65 – 3-D reinforced concrete solid

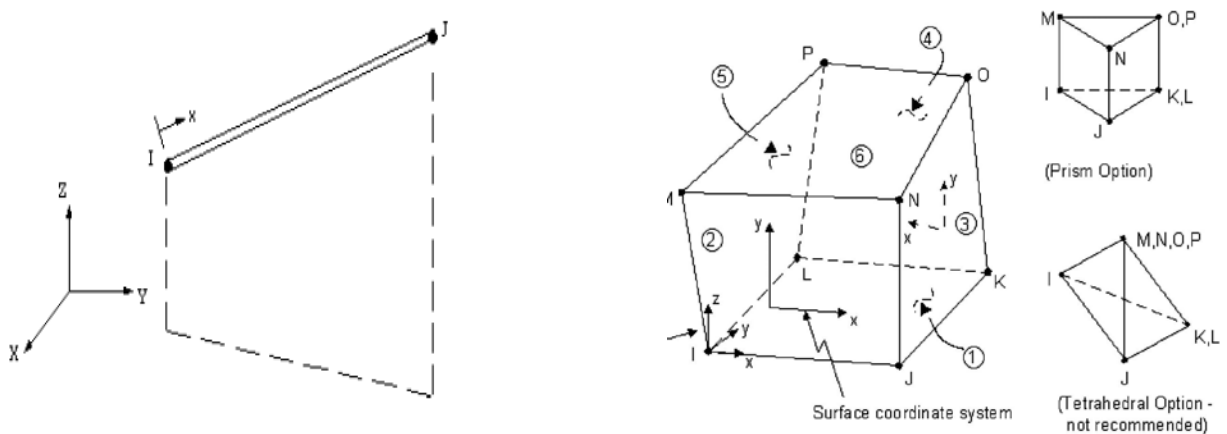


Fig. 3 Link 8 Element

Fig. 4 Solid45 – 3D solid

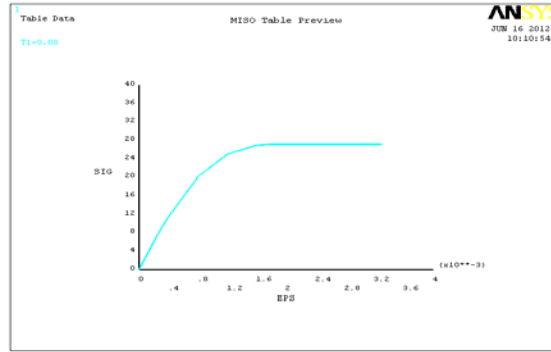


Fig. 5. Uniaxial Stress-Strain Curve of Concrete

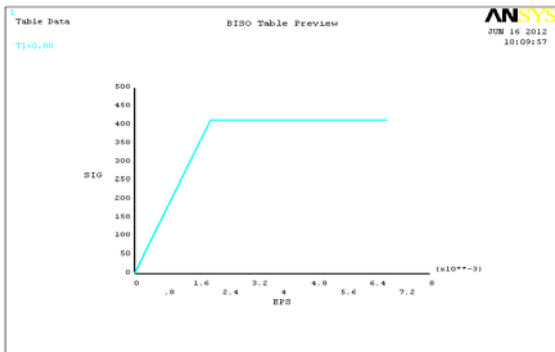


Fig. 6: Idealized Stress-Strain Curve of Main Reinforcing Steel

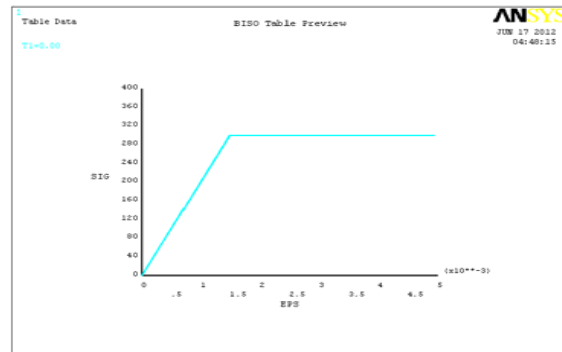


Fig. 7: Idealized Stress-Strain Curve of Web

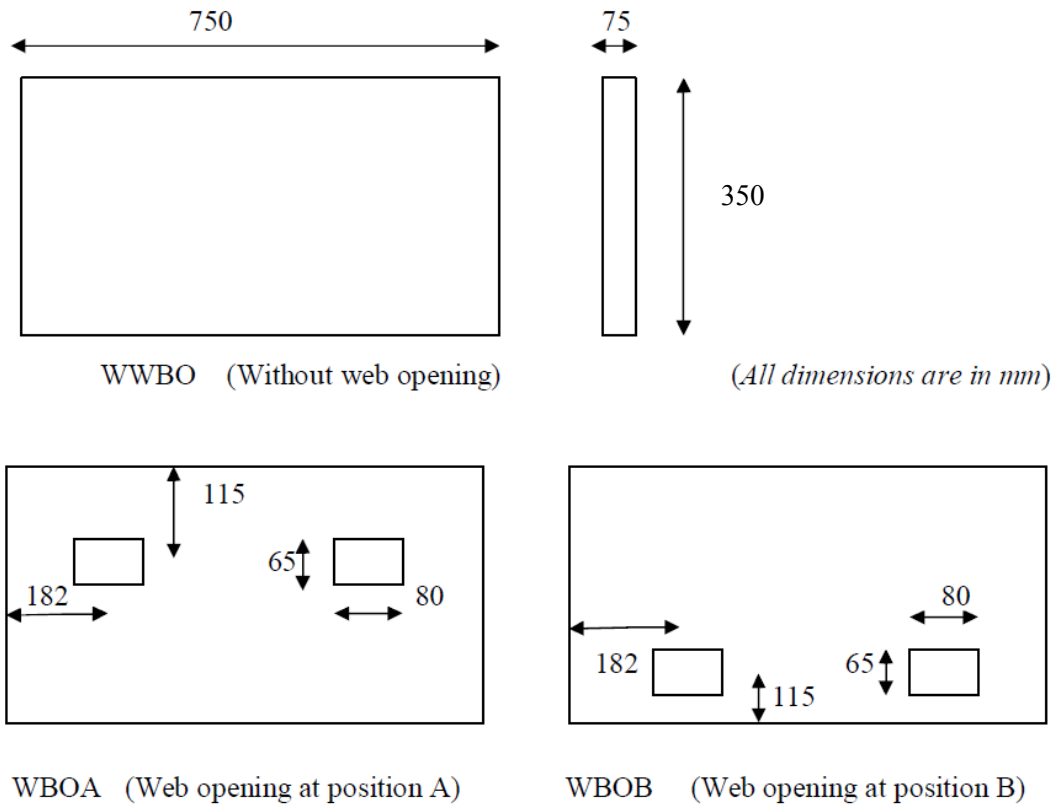


Fig.8 Location Of The Web Opening

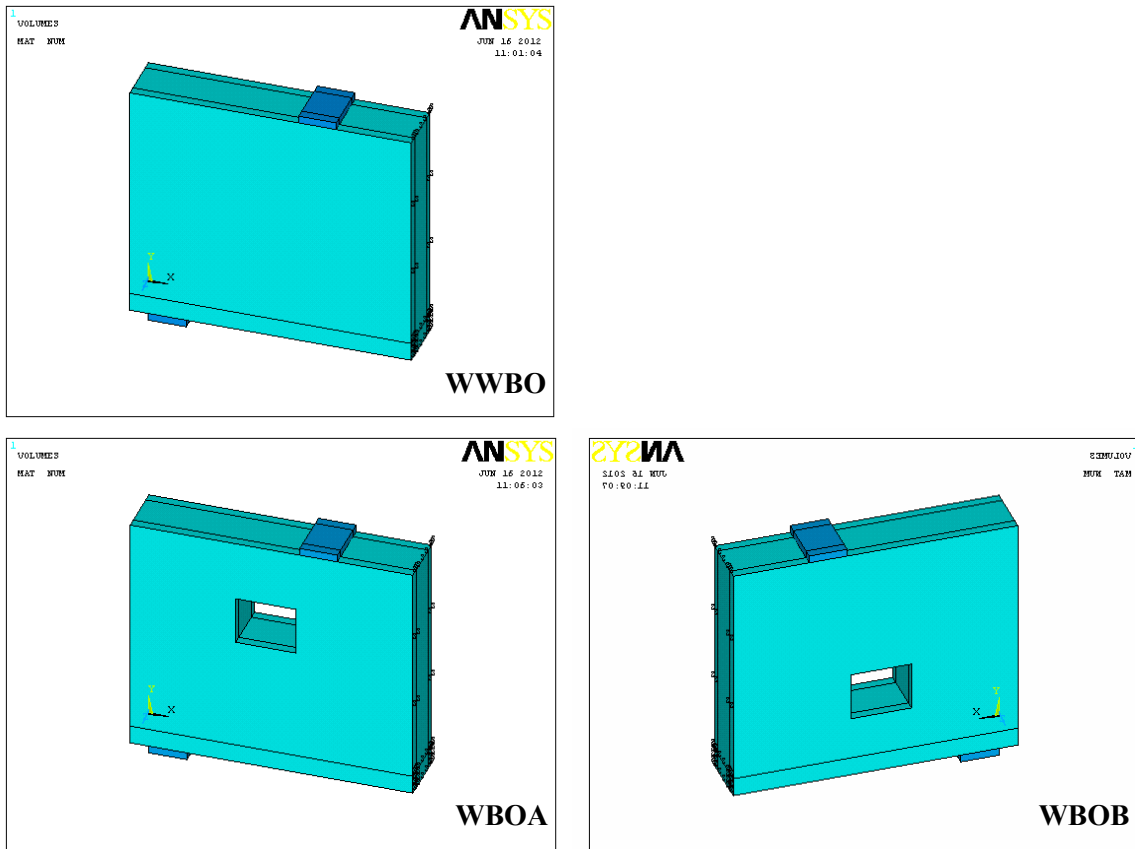


Fig. 9 Modeling Of The Reinforced Concrete Deep Beam

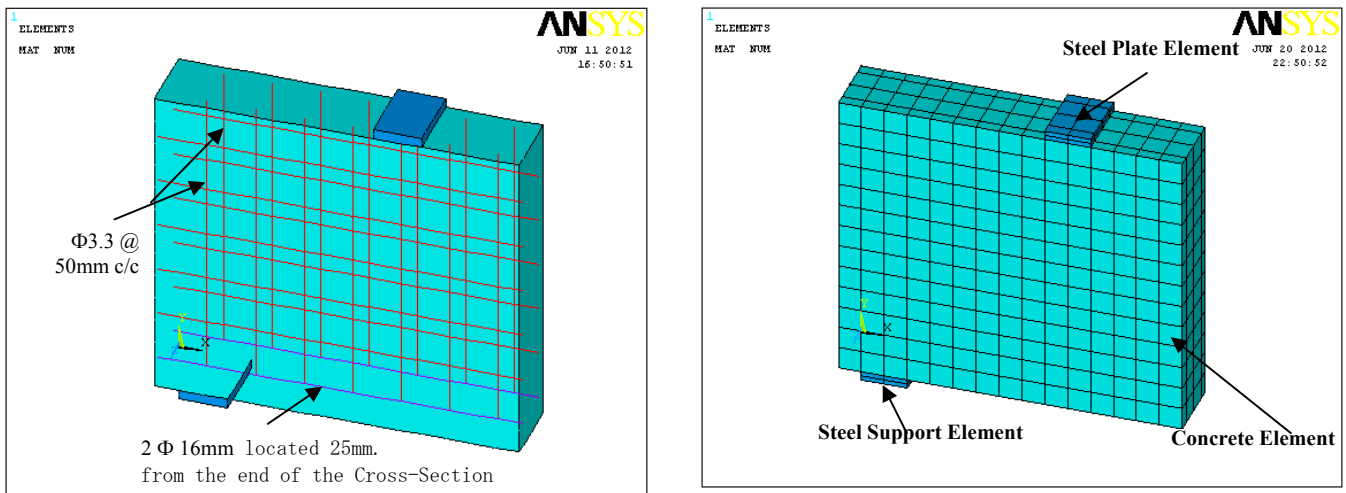


Fig10. Reinforcement Configuration

Fig. 11 Mesh of the Concrete, Steel Plate, and Steel Support

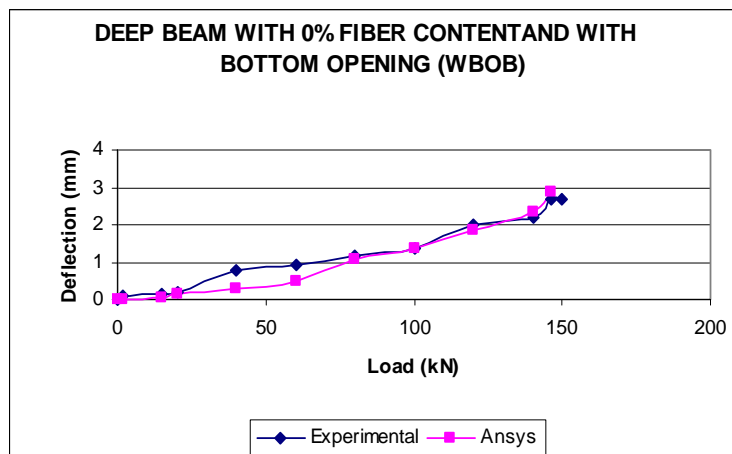
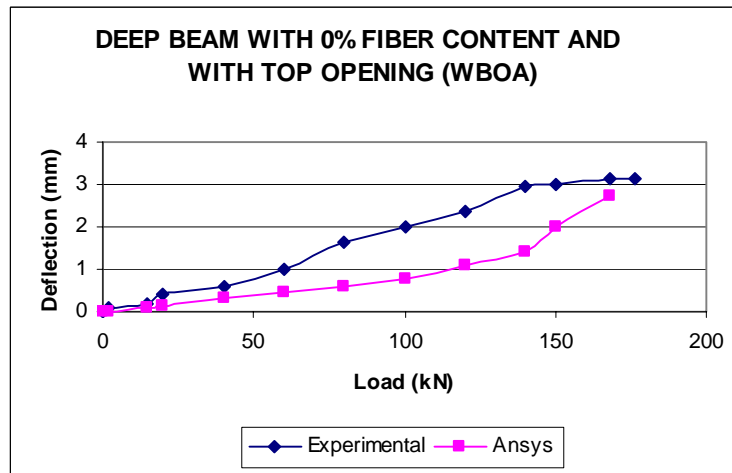
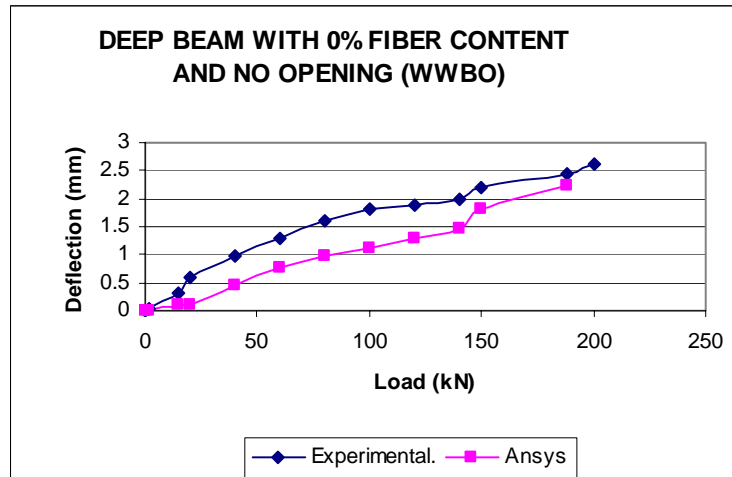


Fig.12 Deep Beam With 0% Fiber Contents With and Without Opening

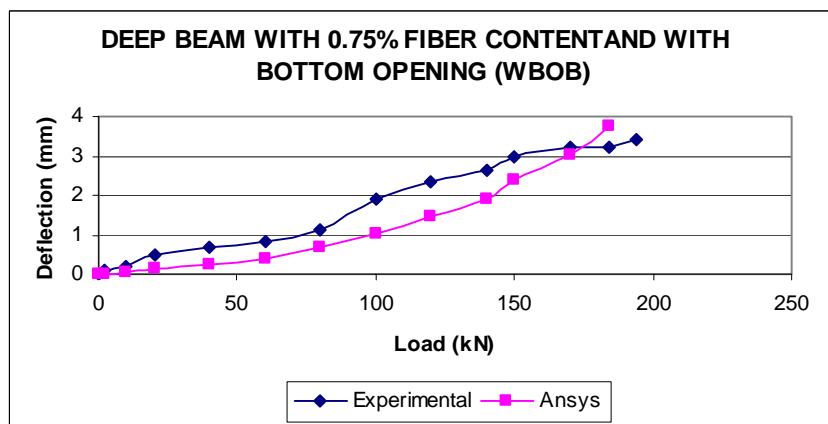
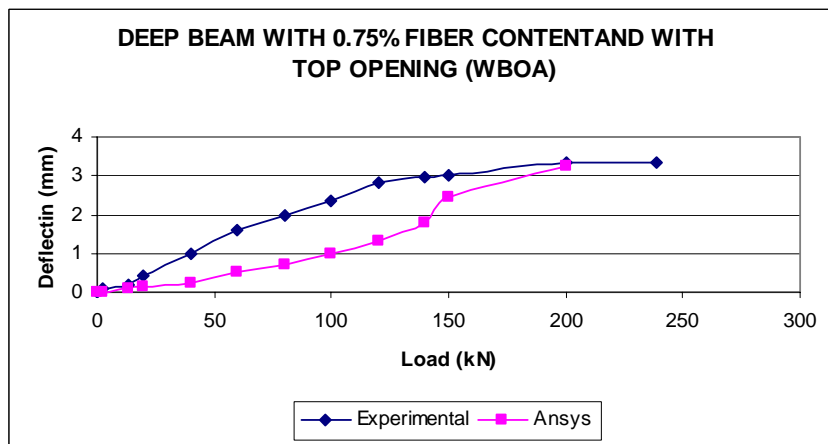
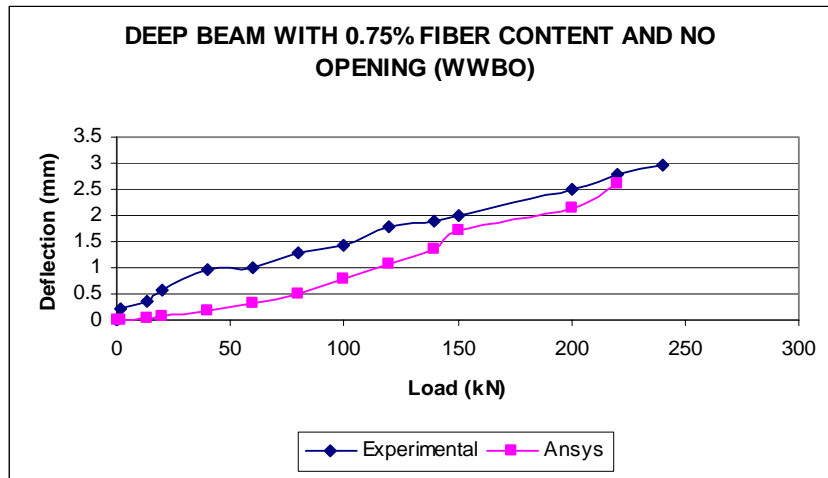


Fig. 13 Deep Beam With 0.75% Fiber Contents With and Without Opening

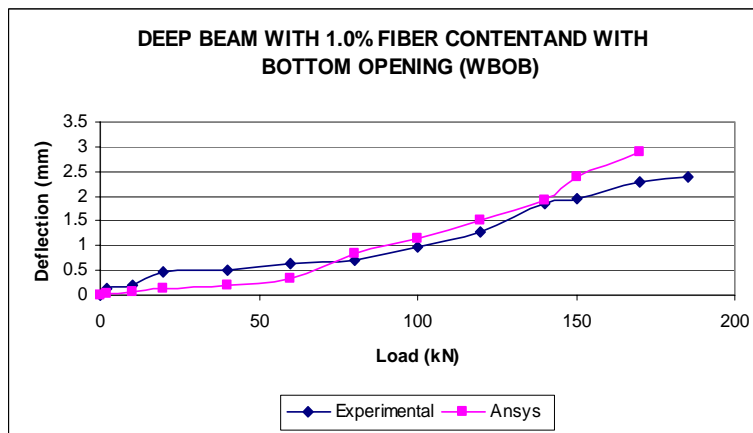
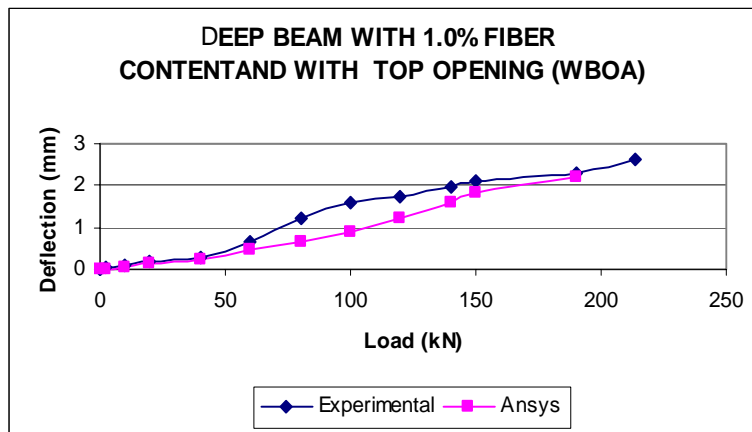
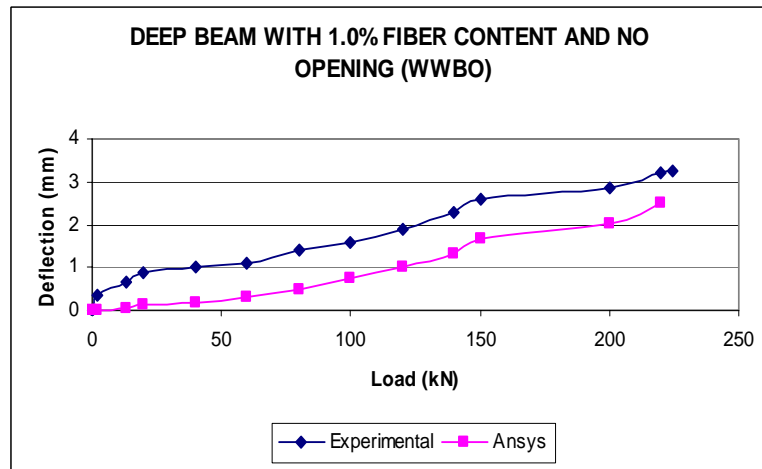


Fig.14 Deep Beam With 1.0% Fiber Contents With and Without Opening

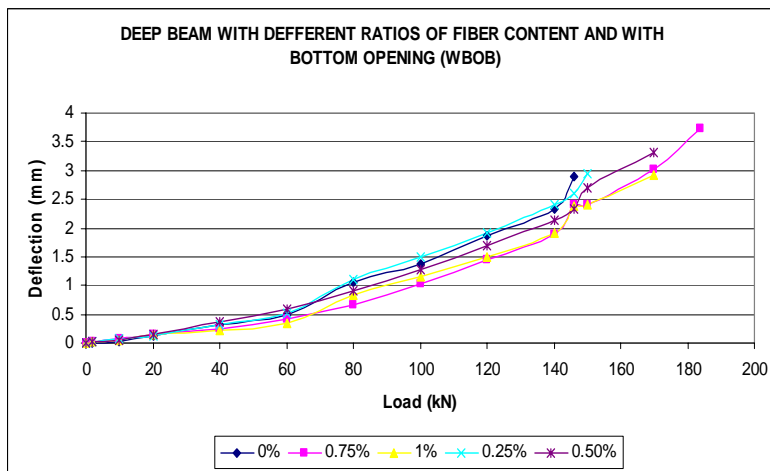
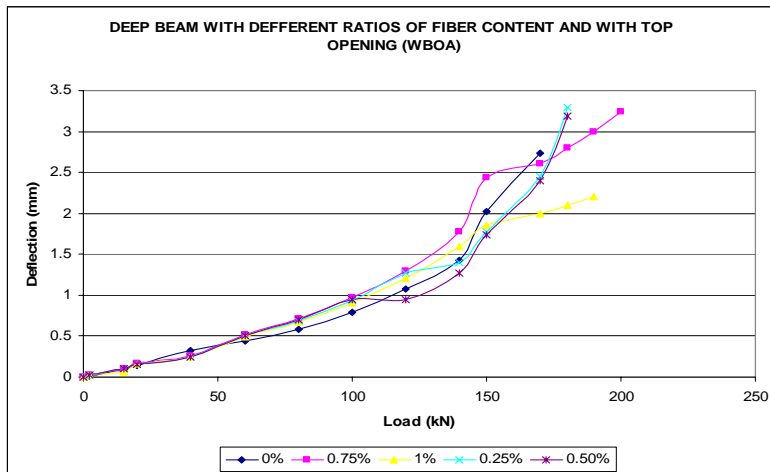
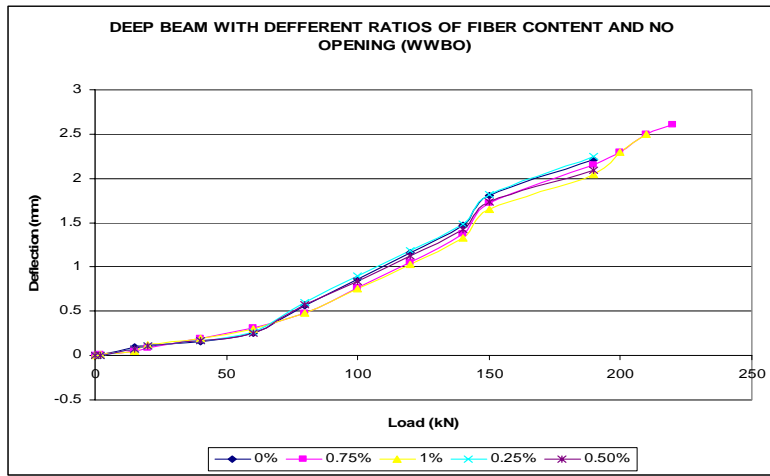


Fig.15 Deep Beam with Different Ratios of Fiber Contents With and Without Opening

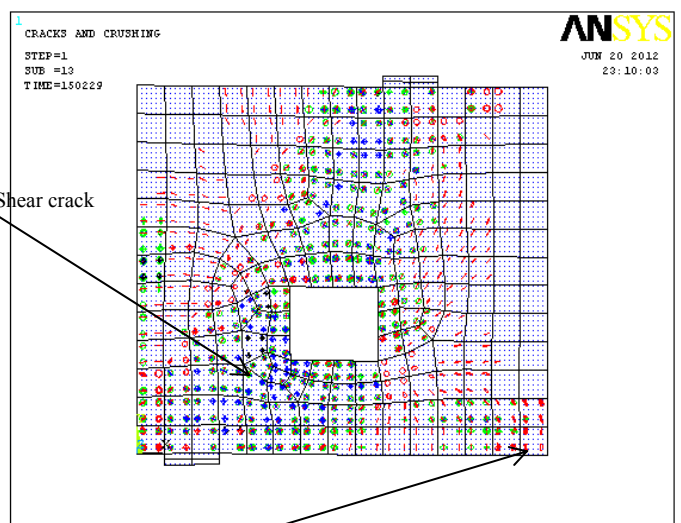
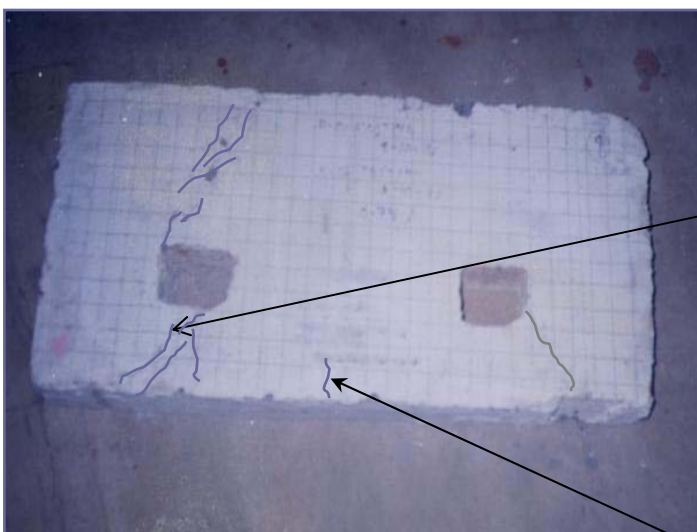
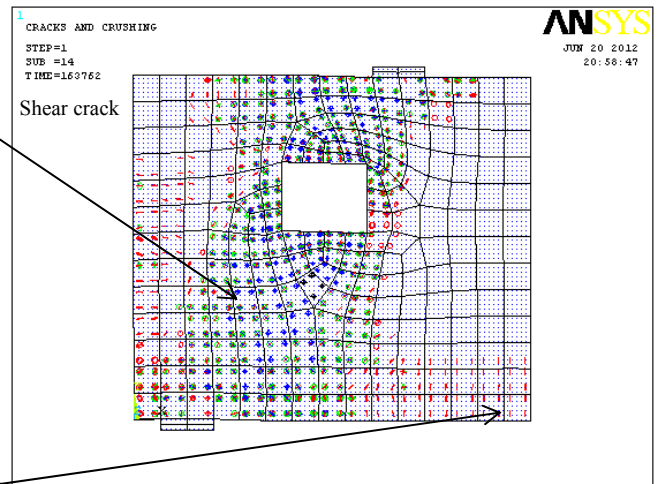
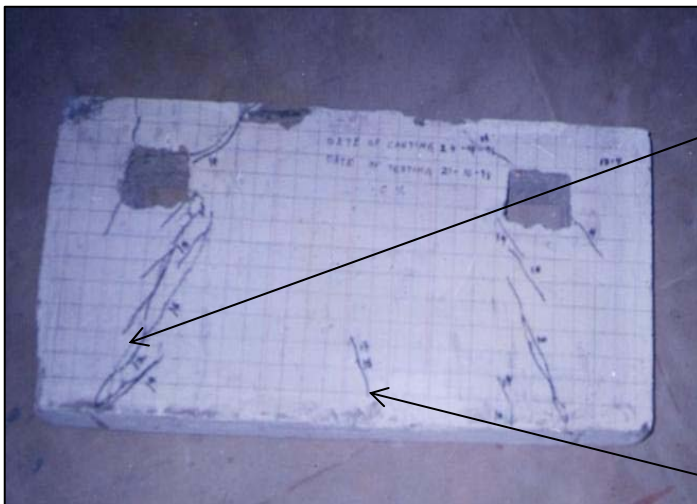
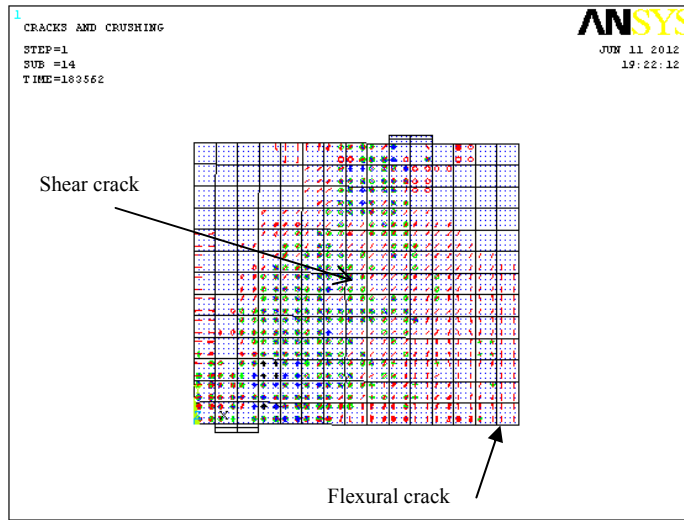
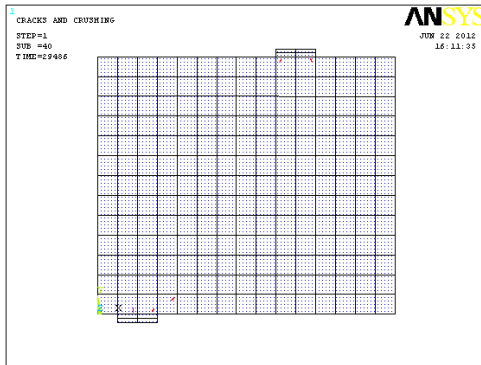
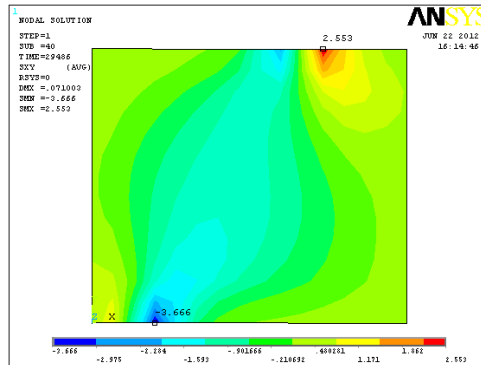


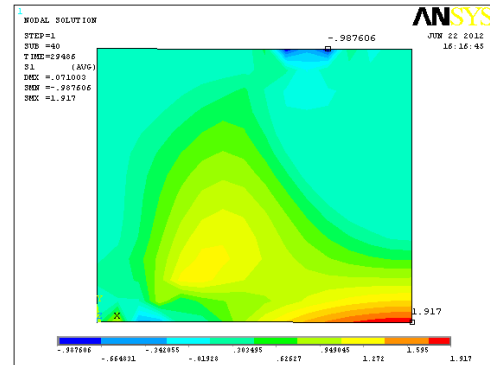
Fig.16 Cracks and Crushing at Ultimate load



a) 1st Crack of WWBO

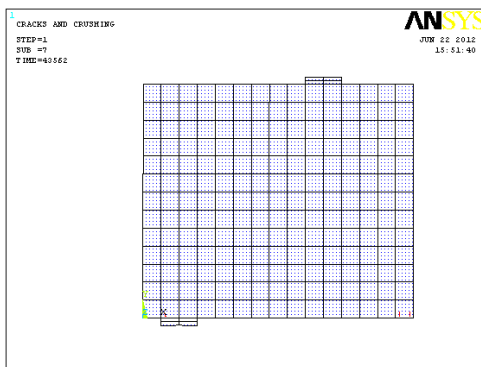


b) Shearing stress of WWBO along XY

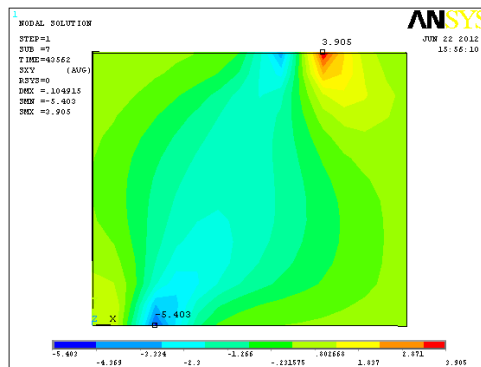


c) The first principal stress of WWBO

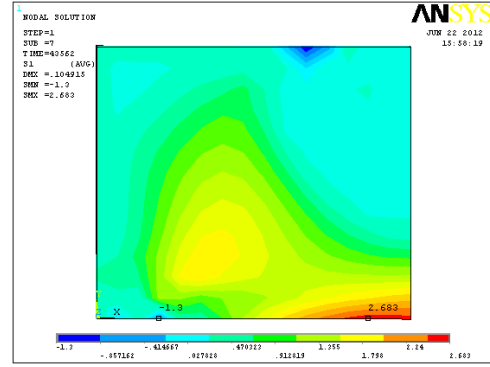
Fig. (17) 1st Crack, Shearing and Principal Stresses for WWBO at 0% Steel Fiber



a) 1st Crack of WWBO

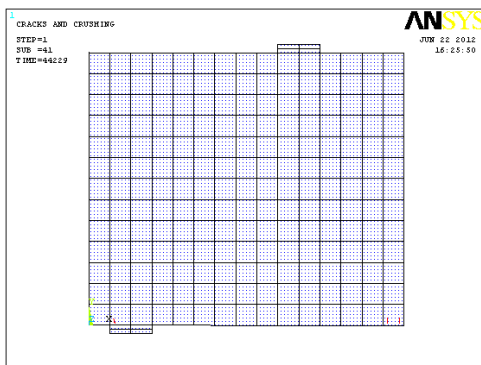


b) Shearing stress of WWBO along XY

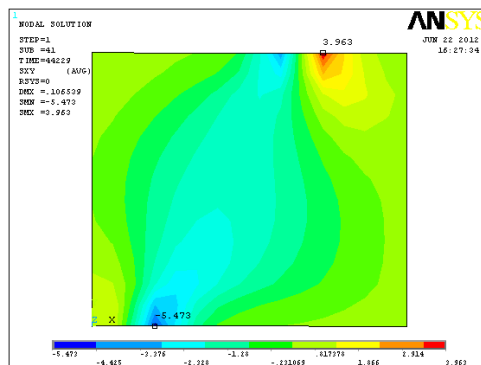


c) The first principal stress of WWBO

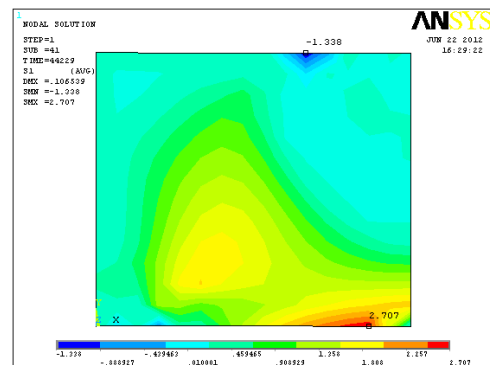
Fig. (18) 1st Crack, Shearing and Principal Stresses for WWBO at 0.75% Steel Fiber



a) 1st Crack of WWBO

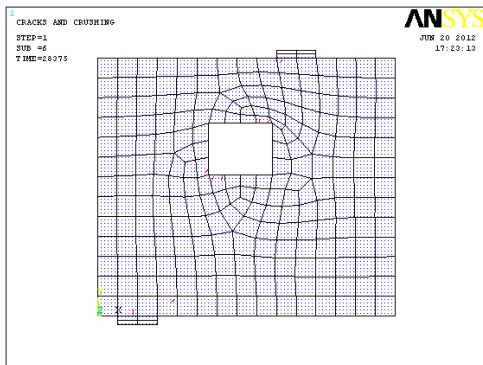


b) Shearing stress of WWBO along XY

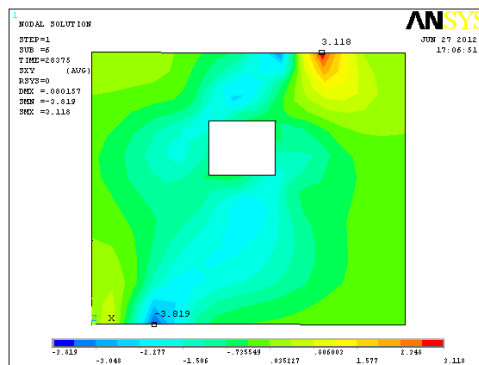


c) The first principal stress of WWBO

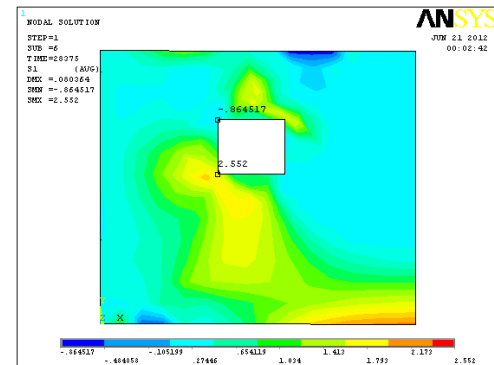
Fig. (19) 1st Crack, Shearing and Principal Stresses for WWBO at 1.0 % Steel Fiber



a) 1st Crack of WBOA

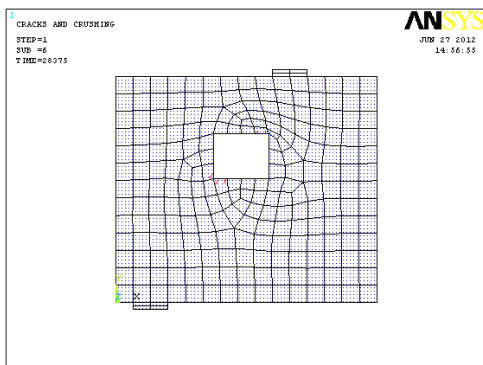


b) Shearing stress of WBOA along XY

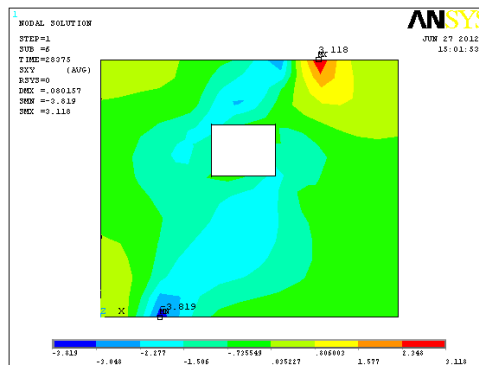


c) The first principal stress of WBOA

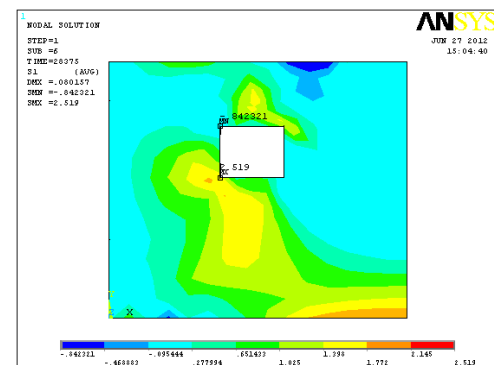
Fig. (20) 1st Crack, Shearing and Principal Stresses for WBOA at 0 % Steel Fiber



a) 1st Crack of WBOA

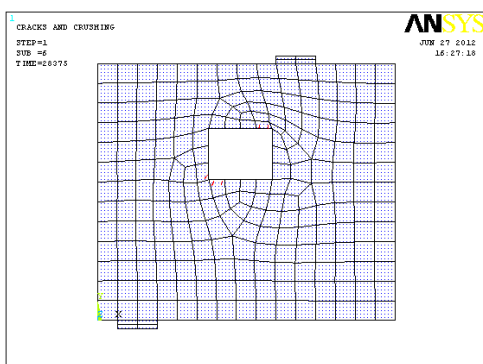


b) Shearing stress of WBOA along XY

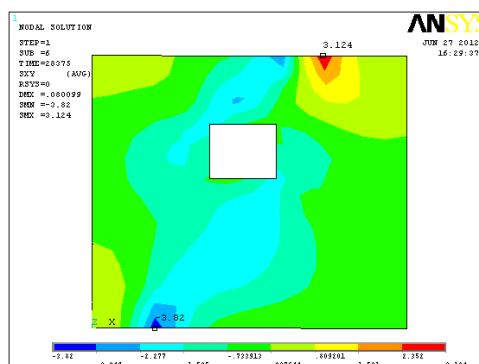


c) The first principal stress of WBOA

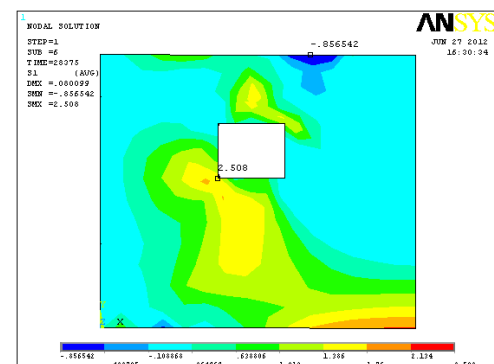
Fig. (21) 1st Crack, Shearing and Principal Stresses for WBOA at 0.75 % Steel Fiber



a) 1st Crack of WBOA

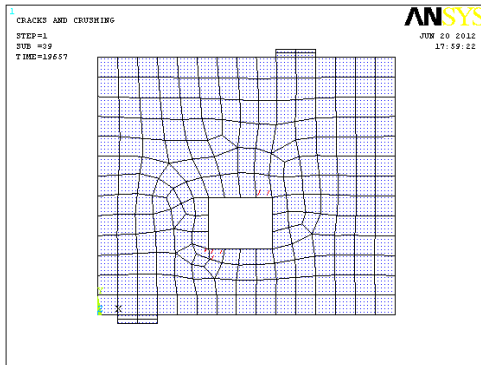


b) Shearing stress of WBOA along XY

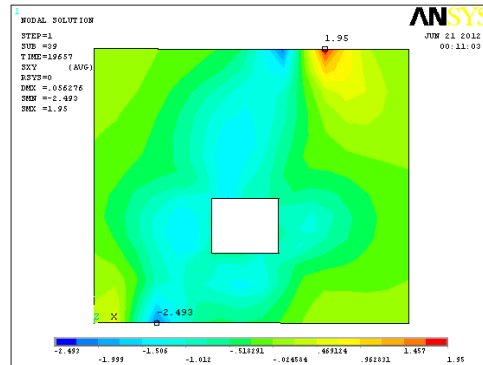


c) The first principal stress of WBOA

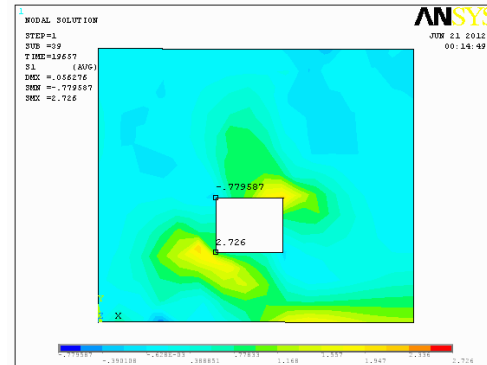
Fig. (22) 1st Crack, Shearing and Principal Stresses for WBOA at 1.0 % Steel Fiber



a) 1st Crack of WBOB

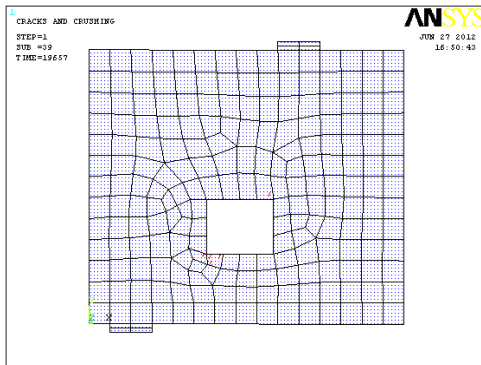


b) Shearing stress of WBOB along XY

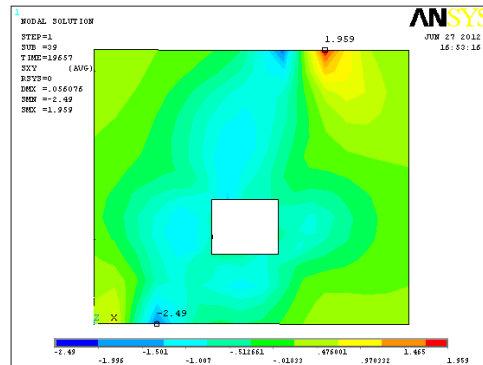


c) The first principal stress of WBOB

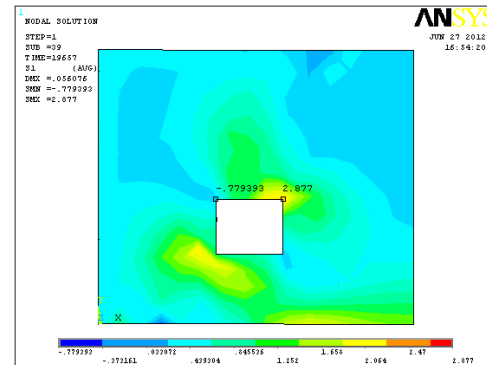
Fig. (23) 1st Crack, Shearing and Principal Stresses for WBOB at 0 % Steel Fiber



a) 1st Crack of WBOB

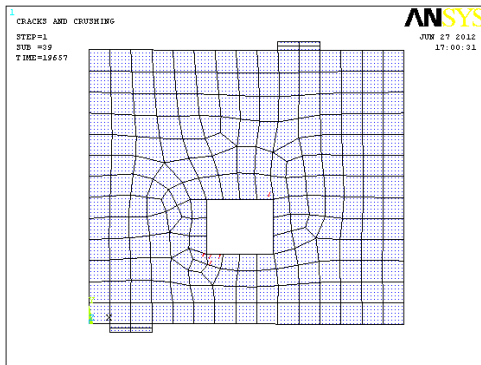


b) Shearing stress of WBOB along XY

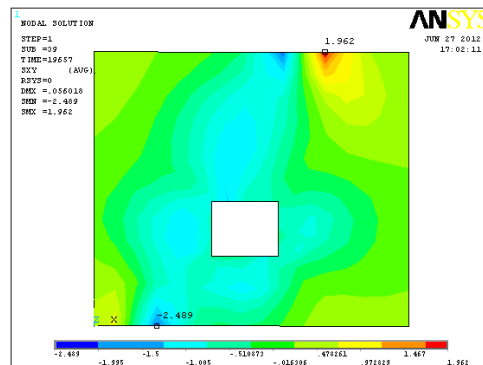


c) The first principal stress of WBOB

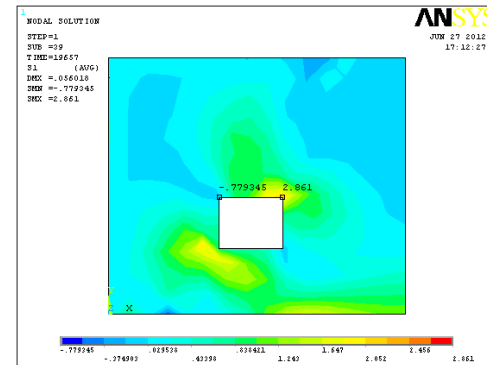
Fig. (24) 1st Crack, Shearing and Principal Stresses for WBOB at 0.75 % Steel Fiber



a) 1st Crack of WBOB



b) Shearing stress of WBOB along XY



c) The first principal stress of WBOB

Fig. (25) 1st Crack, Shearing and Principal Stresses for WBOB at 1.0 % Steel Fiber